Astron. Nachr. / AN **333**, No. 9, 854 – 862 (2012) / **DOI** 10.1002/asna.201211733

The GREGOR polarimetric calibration unit

A. Hofmann[1,⋆], **K. Arlt**[1], **H. Balthasar**[1], **S.M. Bauer**[1], **W. Bittner**[1], **J. Paschke**[1], **E. Popow**[1], **J. Rendtel**[1], **D. Soltau**[2], and **T. Waldmann**[2]

[1] Leibniz-Institut für Astrophysik Potsdam, An der Sternwarte 16, 14482 Potsdam, Germany
[2] Kiepenheuer-Institut für Sonnenphysik, Schöneckstr. 6, 79104 Freiburg, Germany

Received 2012 Aug 27, accepted 2012 Sep 27
Published online 2012 Nov 2

Key words instrumentation: polarimeters – Sun: magnetic fields – techniques: polarimetric

The new Solar telescope GREGOR is designed to observe small-scale dynamic magnetic structures below a size of 70 km on the Sun with high spectral resolution and polarimetric accuracy. For this purpose, the polarimetric concept of GREGOR is based on a combination of post-focus polarimeters with pre-focus equipment for high precision calibration. The Leibniz-Institute for Astrophysics Potsdam developed the GREGOR calibration unit which is an integral part of the telescope. We give an overview of the function and design of the calibration unit and present the results of extensive testing series done in the Solar Observatory "Einsteinturm" and at GREGOR.

1 Introduction

Spectro-polarimetric measurements strongly depend on the spatial, temporal, and spectral resolution as well as the photometric/polarimetric accuracy. The principal task is to find trade-offs between these parameters adapted to the specific objectives of the observations. At GREGOR, this can be realized by an optimum relationship between the intensity of light and the sampling. A high photon flux is needed to reach a large signal-to-noise ratio. With an aperture of 1.5 m GREGOR has a diffraction limited resolution of about 0.″1 at 600 nm. For spectropolarimetry with a spatial resolution of 0.″14 (100 km at the Sun) as planned by the GFPI (see below) we have an intensity of light exceeding that of a diffraction limited telescope by about 50 %. Compared to the neighbouring 70 cm Vacuum Tower Telescope, GREGOR delivers four times more photons to the focal plane (see also Schmidt et al. 2012). This high photon flux enables a high signal to noise ratio for polarimetric purposes.

Taking benefit from these facts, polarimetric measurements at GREGOR will be based on several instrumentations which are optimized to specific spectral ranges or scientific objectives, respectively:

- The GREGOR Fabry-Pérot Interferometer (GFPI) enables imaging spectropolarimetry in a spectral range of 580–660 nm with a theoretical spectral resolution ($\lambda/\Delta\lambda$) of 2.5×10^5 and a spatial resolution of up to 0.″14 (Puschmann et al. 2012).
- The GREGOR Infrared Spectrograph (GRIS) is designed for spectropolarimetry in a spectral range of 1000 to 2200 nm along a slit of $0.''25\times67''$ (Collados et al. 2012).
- The GREGOR polarimetric calibration unit (GPU) is designed and built in the Leibniz-Institute for Astrophysics Potsdam (AIP). It will be an integral part of GREGOR to support accurate polarimetry with GRIS, the GFPI or any other post-focus polarimeter.

The Stokes vector measured by the polarimeter depends on the properties of the telescope and the performance of the polarimeter and is given by $\boldsymbol{S}_{\mathbf{meas}} = \mathbf{X}\cdot\mathbf{T}\cdot\boldsymbol{S}_{\mathbf{Sun}}$ where $\mathbf{X}$ describes the response of the polarimeter, $\mathbf{T}$ is the Mueller matrix of the optical train upstream from the polarimeter, and $\boldsymbol{S}_{\mathbf{Sun}}$ is the Stokes vector incoming from the Sun. The polarimetric accuracy depends significantly on the exact knowledge of $\mathbf{X}$ and $\mathbf{T}$. In general, an experimental determination of these matrices is realized by calibration optics consisting mostly of a combination of a rotatable polarizer and an independently rotatable retarder feeding known states of polarized Stokes vectors into the system as calibration input and measuring the response of the system. For the most polarimeters $\mathbf{X}$ can be regarded as static and is measured by calibration optics in front of the polarimeter.

The situation is more complex for the optical train upstream of the polarimeter. It has a variable configuration and because of the limited aperture of high-precision calibration optics there is no possibility of a full-aperture calibration in front of the telescope. The main contribution to the matrix $\mathbf{T}$ is produced by instrumental polarization due to reflections at mirrors and depends strongly on the angle of reflection. It is virtually zero at normal incidence but reaches substantial values as it deviates from normal incidence. The optical design includes at first an axial-symmetric 3-mirror configuration (M1, M2, and M3) forming a double Gregory system (see Soltau et al. 2012). A field stop at the location of the primary image deflect the most of the light (and heat) out of the telescope and transmits a circular field-of-view with a diam-

⋆ Corresponding author: ahofmann@aip.de

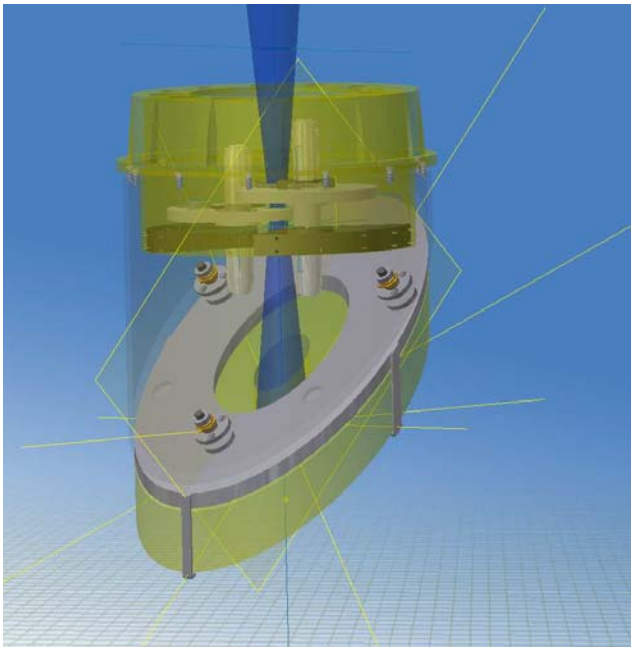

Fig. 1 (online colour at: www.an-journal.org) Constructional sketch showing the unit (green) in the shadow of the Nasmyth mirror (below). Blue: the beam with the focus F2 just at the position of the unit

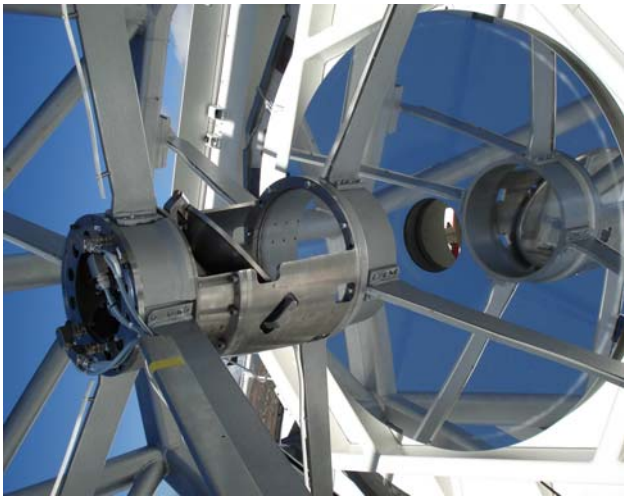

Fig. 2 (online colour at: www.an-journal.org) Position of the calibration unit next to the Nasmyth mirror M4 using the narrow beam close to the secondary focus F2, before the beam is reflected into the coudé axis.

eter of 300″ towards the secondary focus F2 (see Soltau et al. 2012). To this point the beam is rotationally symmetric and the telescope can be regarded as polarization free at a 10^{-4} level (Sánchez Almeida & Martínez Pillet 1992). This suggests to locate the polarization the calibration unit there nearby to the Nasmyth mirror M4 and using the narrow beam close to the secondary focus F2 (see Soltau et al. 2012) as shown in Fig. 1.

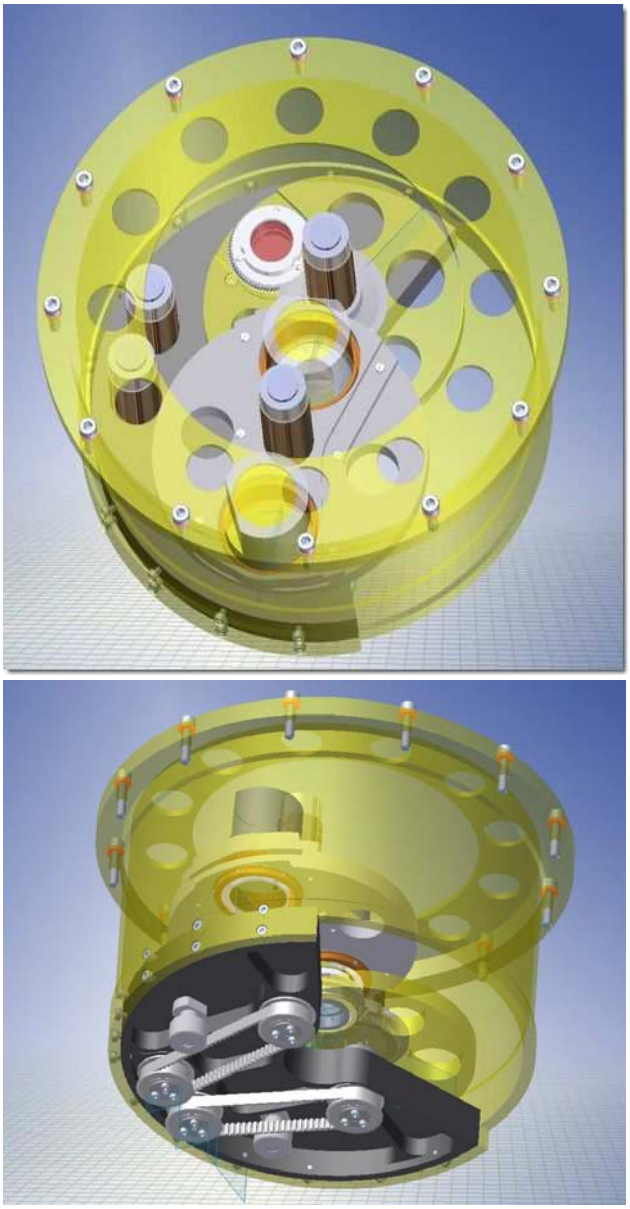

Fig. 3 (online colour at: www.an-journal.org) Constructional sketches of the unit. *Top*: front view showing the two wheels to insert and rotate different calibration optics into the beam. There are four micromotors (black cylinders) situated at the left hand to rotate the wheels and at the center of the wheels to rotate the mounts, respectively. *Bottom*: back view showing the gear belts and drives of the wheels

.

Some partial results of design and construction of the GPU were already described in different progress reports (e.g. Hofmann 2008; Hofmann, Rendtel & Arlt 2009). Here we give a total review of all important aspects of the GPU after its integration into the GREGOR telescope.

2 Functions, design and construction, control

2.1 Functions

The main function of the GPU is to calibrate any post-focus polarimeter. For this reason it has to fulfill two tasks: (i) it takes into consideration the instrumental polarization induced by optical components between the calibration optics and the polarimeter; (ii) it calibrates the performance of the polarimeter. For further test and adjustment purposes, the GPU provides additional functions. In the non-polarimetric mode, a free aperture and a 60 μm pinhole are available. The latter allows, for example, the adjustment of the adaptive optics system (see Berkefeld et al. 2012). In the polarimetric mode, components of the calibration optics can be placed in the beam and can be rotated according to the requirements of the calibration scheme. In both modes, a 0.5 mm reticle for scale determination and alignment is available.

2.2 Design and construction

Figure 2 shows the GPU mounted in front of the M4-unit which was also designed and constructed in the AIP and enables an exact adjustment of the Nasmyth-mirror M4 in shift and tilt by increments of 0.5 μm.

The different functions of the calibration unit are implemented by devices mounted on two rotatable wheels (see Fig. 3) which carry all the needed optical components in precision mounts. The wheels are driven by DC-micromotors IGR 2224-22.5-IE2-512 of the Faulhaber GmbH (Schönaich, Germany) and can be rotated via gear belts by increments of about $9\farcs15$ (1 step).

There are two rotation mounts and two free apertures in the front wheel. The rotation mounts can be rotated by increments of $5\farcs5$. One contains the linear polarizer, the second is (differently to the constructional sketch in Fig. 3) still empty. The front-side plane of the second wheel is at the position of F2. This wheel contains also two rotation mounts with the retarders for the visible and infrared spectral ranges, two fixed mounts with the pinhole and the 0.5 mm grid (target), and two free apertures. The free aperture of 20 mm diameter is for free beam-transmission, the other of 25 mm diameter is equipped with a reticle and can be used to implement further optics. The two retarders can be rotated by increments of $9\farcs15$.

2.3 Controlling

The control software for the GPU is implemented in LabView 8.0. It offers a graphical user interface (GUI) and an interface to the GREGOR communication protocol (DCP).

The DCP interface of the control software listens to the DCP server, and it can be used to control the GPU remotely, e.g. by commands generated and sent by post focus instruments such as the FPI etc. Basically, all functionality that can be addressed by the GUI can also be addressed via the DCP interface. This allows for remote control of the GPU when calibration procedures are carried out.

The GUI as the user interface consists of two panels. The first Main Panel (left panel in Fig. 4) offers two radio button lists that can be used to insert the optical elements of the two rotating wheels into the light beam, and to rotate the optical instruments that are positioned in the light beam, if they are rotatable. The second panel (right panel in Fig. 4) is called the Axes/Status Panel. It shows the status of the individual axes (referenced / not referenced), and the status of the connection to the DCP server as well as the status of the connection to the XPort. It also holds control elements that can be used to rotate the individual axes.

Commands, received by the DCP client or generated by the user interface, are ASCII strings and they are processed by the execution part of the control program into axis relevant instructions, also ASCII strings. They are sent by TCP/IP communication protocol to a XPort, which corresponds with a controller to a CoSM field bus systems transferring the the instruction to each of four axes.

3 Testing the calibration optics

3.1 The calibration optics

The calibration optics consist of a linear polarizer (rotatable) and two achromatic quarter-wave plates (rotatable) which are in use alternatively for observations in the visual or the infrared range. However, the power density of about 40 W cm^{-2} and the large cone angle of the beam ($\pm5\fdg8$) cause extreme conditions for polarimetry that require a new way for the calibration optics.

An air spaced Marple-Hess prism (specific configuration of a double Glan-Taylor prism, designed by B. Halle Nachfl. Gmbh, Berlin, Germany) is used as linear polarizer to withstand the power density and to perform the required high distinction ratio of at least 10^{-5}. The prism is constructed from calcite and has an angular acceptance of $\pm5^\circ$ over the spectral range of 350–1600 nm.

Combined zero-order wave plates of polymethylmetacrylat (PMMA) were designed by Astropribor (Kiev, Ukraine) as superachromatic retarders. The retarders are constructed as five-component wave plates with an angular acceptance of $\pm7^\circ$, a temperature range of $-20\,^\circ$C to $50\,^\circ$C and a damage threshold of 500 W cm^{-2} CW. Contrary to quartz and MgF_2-plates these are nearly free of polarized spectral fringes which is important for high-resolution spectropolarimetry. More information can be found in Samoylov et al. (2004).

For test measurements the GPU was placed in front of the spectrograph slit in the laboratory of the Solar Observatory Einsteinturm in Potsdam. The Littrow spectrograph has a focal length of 12 m and a spectral resolution ($\lambda/\Delta\lambda$) of 1.03×10^6 in its fourth order mostly used.

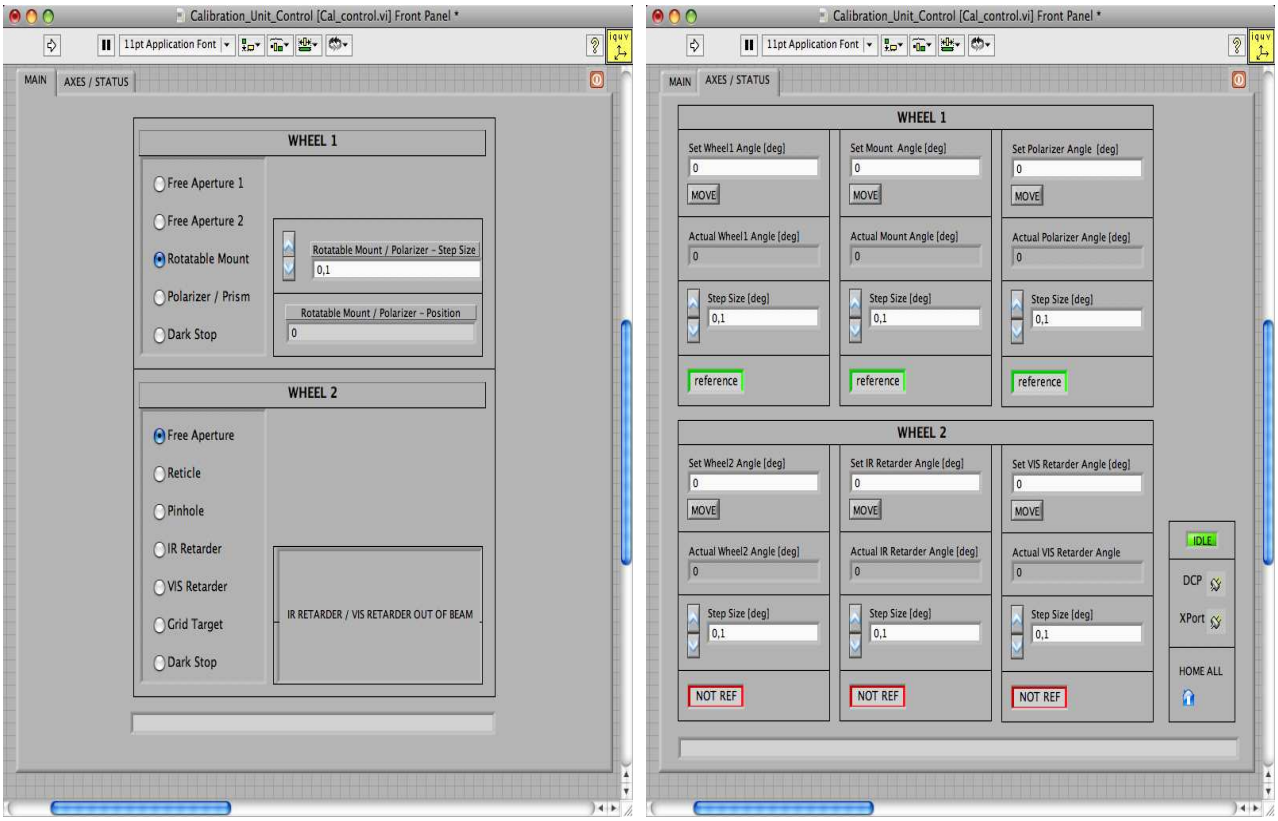

Fig. 4 (online colour at: www.an-journal.org) The two GUI-tabs of the control software.

3.2 The linear polarizer (prism)

To test the prism, two linear polarizers adjusted for maximum transition were mounted behind or in front of the GPU, respectively. Thus, the prism can be rotated in linear polarized light and the measured intensity does not depend on any linear polarization of the light source or the sensitivity of the spectrograph against any linear polarization. The variation of the intensity depends only on the rotation angle φ. With $\mathrm{S2} = \sin 2\varphi$ and $\mathrm{C2} = \cos 2\varphi$, the intensity variation is given by

$$I' = 0.25\,[(k_1 + k_2) + 2(k_1 - k_2)\mathrm{C2} + (k_1 + k_2)\mathrm{C2}^2 + 2k_1k_2\,\mathrm{S2}^2]\,I_0\,. \quad (1)$$

Rotating the prism over a range of $360°$ yields two maxima and two minima of intensity. Two of these are shown in Fig. 5. The lower plot deviates somewhat from the expected $\cos^2$-curve because it is flattened due to nonlinearity of the detector at low intensities. The measured intensity variations can be used to determine the parameters k_1 and k_2 of maximum and minimum transmission. With $k_1 = 116454$ and $k_2 = 0.225$ we achieve an extinction ratio of $\mathrm{er} = k_2/k_1 \approx 2{\times}10^{-6}$ or a contrast ratio of $\mathrm{cr} = k_1/k_2 \approx 500000 : 1$.

3.3 The retarders (wave plates)

For combined zero-order retarders, the position of the fast axis varies with the wavelength. This was measured by the standard method for circular retarders, i.e., rotating the retarder between parallel linear polarizers. The observed intensity is described by

$$I' = 0.5\,[1 - 1/2 \cdot \sin^2 2\varphi \cdot (1 - \cos\delta)]\,I_0, \quad (2)$$

where φ is the rotation angle and δ is the retardance. The intensity curve shows maxima when the fast or slow axis are parallel ($\varphi = n \cdot \pi/2$) to the transmission axes of the polarizers and, consequently, minima when they are $45°$ between these positions. The procedure is symmetrical by $180°$, and, in principle, a rotation over a $180°$ range would be sufficient. However, we rotated the retarders by a full circle (i.e., 72 intensity measurements per wavelength point) to compensate for residual effects of beam wobble and to double the number of values included in the calculation of the position angle and retardance. Each of these data sets defines four maxima and four minima.

The positions and intensity values of all extrema were determined by parabolic fits. Measurements were performed in the ranges 379 nm–980 nm (retarder for the visible range) and 656–1105 nm (retarder for the IR-range), respectively. The variation of the position angle is shown

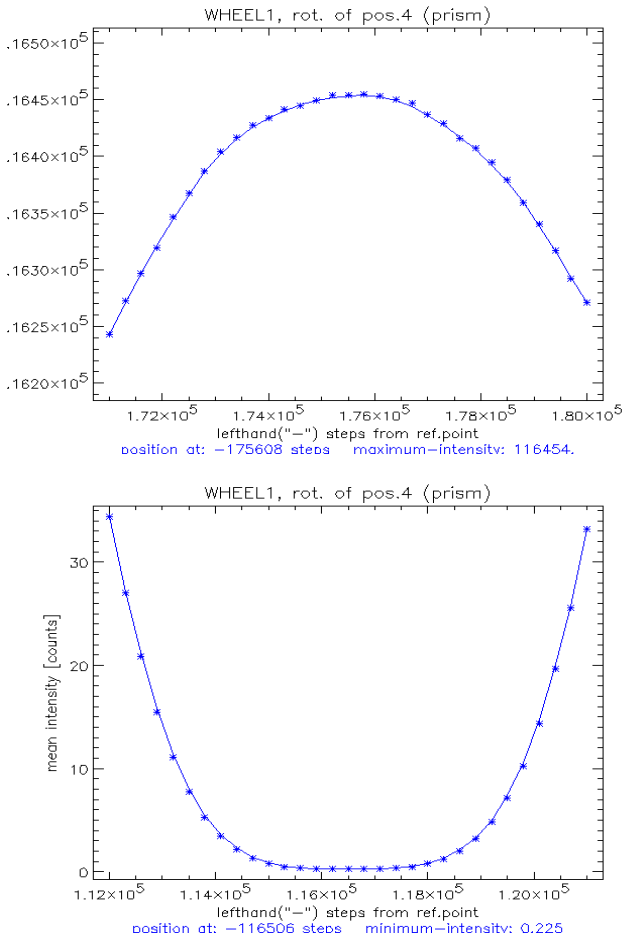

Fig. 5 (online colour at: www.an-journal.org) Intensities for rotating the prism in linear polarized light. *Top*: rotation around maximum transition; *bottom*: rotation around minimum transition.

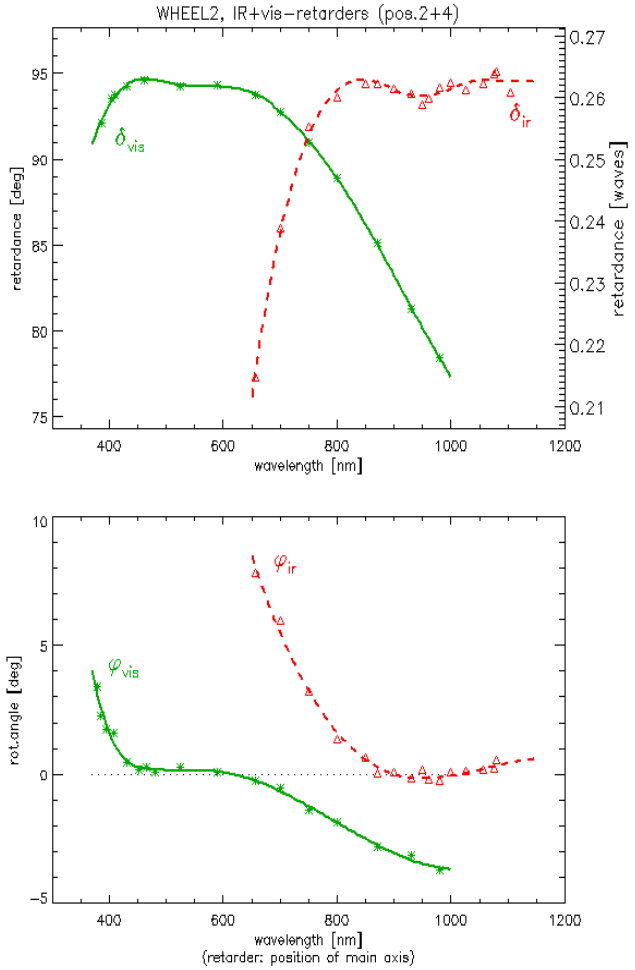

Fig. 6 (online colour at: www.an-journal.org) Wavelength dependence for parameters of the retarders (i) for the visible (green symbols represent the measurements and the solid lines are splines between them) and (ii) for the infrared (red symbols and dashed lines) spectral ranges. *Top*: retardanc, *bottom*: orientation of the fast axis.

in the lower part of Fig. 6. The ratio between the average of the minima and the average of the maxima is given by $\langle I'_{\min}\rangle \,/\, \langle I'_{\max}\rangle = 0.5\,(1+\cos\delta)$ which can be used to determine the retardances shown in the upper part of Fig. 6.

3.4 Polarimetric performance

The polarimetric throughput of the unit depends on the parameters of the individual components and can be described by the Stokes-vector:

$$\begin{aligned}\boldsymbol{S'}(\varphi_1, k_1, k_2, \varphi_2, \delta) &= (I', Q', U', V') \\ &= \mathbf{G}(\varphi_2, \delta)\ \mathbf{P}(\varphi_1, k_1, k_2) \cdot \boldsymbol{S}, \qquad (3)\end{aligned}$$

where $\boldsymbol{S}$ is the Stokes-vector of the input beam. $\mathbf{P}$ and $\mathbf{G}$ are the Mueller matrices of the polarizer and the retarder, depending on their rotation φ_1 and φ_2 against any reference system and their transmission parameters k_1 and k_2 or retardation δ, respectively. An extensive mathematical description for calculating $\boldsymbol{S'}$ is given in the Appendix. Equations (A6)–(A9) given there can be used to calculate how closely the calibration Stokes vectors produced by the polarization optics match the ideal ones. Figure 7 shows the results for the case that circular polarization (Stokes V) is generated.

The parameters q', u', v' correspond to the fractional polarizations $Q'/I', U'/I'$, and V'/I'. In the left-hand graphs is assumed that the retarder axis is rotated by $45°$ to the maximum transmission of the prism but fixed to one optimum angle over the whole wavelength range. The right-hand graphs show the typical situation in solar physics where the polarimetry is done in a very narrow spectral range, i.e., in this case the retarder is rotated to the $45°$-position of its axis at each wavelength according to the angular behaviour shown in the left part of Fig. 6. This results in $u' = 0$ and only the contribution of Q' remains. The alternative use of two retarders ensures that the parameters are found to be very close to the ideal ones ($v' \equiv 1,\ q' = u' = 0$) over the entire wavelength range. These ideal parameters are reached only at the wavelengths where $\delta = 90°$ (exact quarter-wave retardation).

4 The unit at GREGOR

4.1 A polarimetric telescope model

GREGOR is an alt-azimuthal mounted telescope with the consequence that there are two locations where mirrors rotate against each other or against the post-focus instruments that are installed fixed in the laboratory inside the building, i.e. behind the coudé train (mirrors M5, M6 and M7, see at Soltau et al. 2012). Depending on telescope position, these rotations can be quite fast, and a calibration measurement would not perfectly fit to the observation. Therefore we developed a polarimetric telescope model (cf. Balthasar et al. 2011). Incidence angles on the mirrors and their orientation are known or given by the telescope position. Mueller matrices are calculated for all mirrors, which are coated with aluminium. Aluminium oxidates immediately after coating until the oxide layer is about 4 nm thick. This happens within a few hours, and then the situation becomes stable (cf. van Harten et al. 2009). The polarimetric properties of such a coating are well known (Lide 1993). However, dust and grime cannot be completely avoided, and they affect the complex refractive indices of the mirrors. As reference plane in F2, we define that the positive Q-polarization plane is parallel to the elevation plane of the telescope. Since the reference plane of a single mirror is given by the plane of incidence (cf. Capitani et al. 1989), rotation matrices have to be included. The optical coudé train is enclosed and can be evacuated, therefore we also consider in our model a possible influence of the entrance and exit windows assuming unidirectional stress (cf. Beck at al. 2005). Retardance and polarimetric orientation of these windows are free parameters in the model that have to be determined.

Finally, all these matrices have to be multiplied, and we obtain the following equation:

$$M_{\rm G} = PF \cdot AO \cdot M11 \cdot R10 \cdot D \cdot R7 \cdot W2 \cdot M7 \cdot M6 \cdot M5 \cdot R5 \cdot W1 \cdot M4 \cdot R4 \cdot M3 \cdot M2 \cdot M1 \cdot R1 \quad (4)$$

Mueller matrices of the mirrors are indicated with M and rotation matrices by R. $R1$ gives the rotation from the solar North-South direction to the elevation plane of the telescope. The equation includes the image derotator D which consists of mirrors M8, M9 and M10. Mueller matrices of the AO-train (between F3 and F4) and the optical elements of the post-focus instruments (PF) before the polarimetric modulation have to be measured separately.

The code of the telescope model is written in IDL (Interactive Data Language). Depending on purpose, there are different entries and exits to the code, and the derotator can be omitted. For calibration with the GPU, an entry at F2 is programmed. The telescope model will become part of the GREGOR data pipeline.

4.2 Measurements of the instrumental polarization

The GPU has been used to determine the instrumental polarization of the GREGOR telescope. For this purpose, white light was inserted via fiber in the primary focus F1. A polarimeter consisting of rotatable achromatic half- and quarter-wave plates and a calcite beam splitter was placed on the AO bench next to focus F3. The intensities in the two beams were measured for six different orientations of the phase plates as listed in Table 1. We obtain the Stokes-parameters by either combining the two beams or the two phase plate states that exchange the beams. This procedure allows us to determine the Stokes-parameters in four different ways that are combined for the display in Fig. 8. Statistical errors are smaller than 0.035, and in most cases they are even smaller than 0.01. Therefore error bars in Fig. 8 would be smaller than the symbols. Before, the polarimeter was adjusted in the laboratory. For this purpose, we put a linear polarizer and another quarter-wave plate in front of it and adjusted the phase plates in a way that according to the inserted light one of the intensities of the two beams was minimized. We checked that the two beams had almost equal intensities, when the phase plates were in one of the other positions given in Table 1.

Table 1 Angles of the phase plates representing the six states of the polarimeter.

State	1	2	3	4	5	6
$\lambda/2$	0	22.5	45	67.5	0	0
$\lambda/4$	0	0	0	0	45	135
Stokes par.	$+Q$	$+U$	$-Q$	$-U$	$+V$	$-V$

The instrumental polarization was measured for three different elevation angles of the telescope (0°, 30°, and 60°), for seven azimuth positions (–90°, –60°, –30°, 0°, 30°, 60°, and 90°), and for two wavelengths, 530 nm and 630 nm. Results for 630 nm are shown in Fig. 8. Those for 530 nm are not significantly different. Taking such a data set requires almost a day, since many settings must be done manually. Qualitatively we find a good agreement between measurements and telescope model. Deviations typically smaller than 0.05 (degree of polarization), except for a few telescope positions where a certain setting might have been wrong. Only for the crosstalk from V to Q and U we encounter systematic deviations up to 0.1, but they can be reduced assuming that the parameters of the retarder in the GPU deviated from the ideal values (retardance $88°$ and orientation $43\overset{\circ}{.}5$). During these measurements, the exit window of the coudé-train was not mounted. Assuming unidirectional stress on the entrance window, we found the best results for a retardance of three degrees and an orientation of six degrees by minimizing the deviation between measurements and model (considered in Fig. 8). As another free parameter, we assume a tilt of the polarimeter in its final mount on the vertical AO-bench that we determined to be 8.2 degrees.

Once the computer-controlled GREGOR post-focus polarimeters will be in full operation, it will become much faster to take calibration sets with sufficient independent

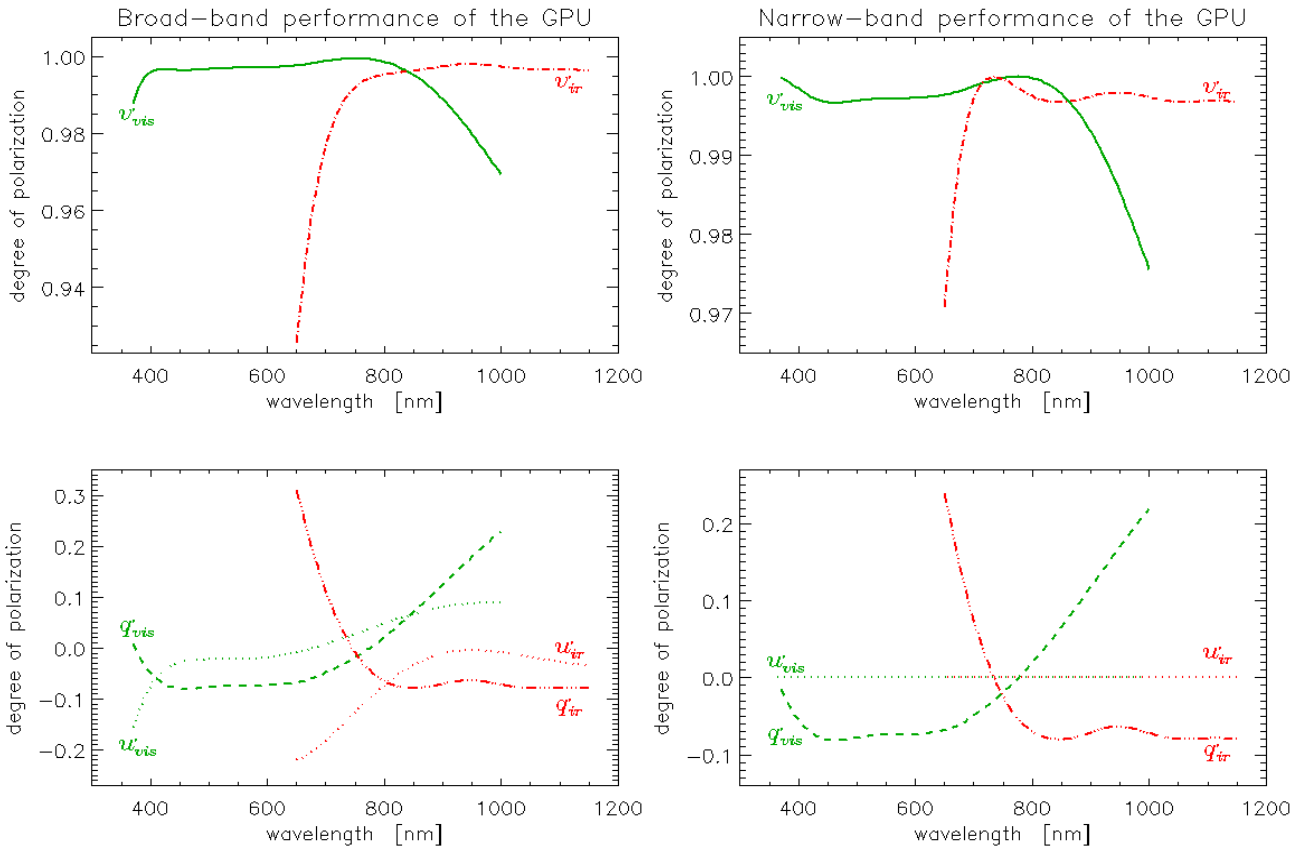

Fig. 7 (online colour at: www.an-journal.org) Wavelength dependence of the performance in generating circular polarized light. Green: using the retarder for the visible range, red: using the retarder for the infrared range.

measurements that will allow to determine also deviations from the nominal specifications of the elements in the calibration unit and automatic fits of the windows of the coudé train (cf. Skumanich et al. 1997; Selbing 2005; Socas-Navarro et al. 2011).

5 Discussion and summary

We tested all optical characteristics of the linear polarizers and retarders in great detail, using the spectral-polarimetric laboratory of the Solar observatory "Einsteinturm" of the AIP. The obtained parameters are very close to the expected calculated values. The deviations between the calibration Stokes vectors and the ideal ones are very small. So the unit suited for different calibration routines to determine the necessary correction matrices: (i) the more classical ones which need only a few measurements assuming ideal calibration Stokes vectors and taking into account the (known) non-ideal parameters of the calibration optics in the calculation process (see, e.g., Jäger & Oetken 1963) or (ii) those which take larger data sets and includes also the determination of the parameters of the optics in the calibration routine (see, e.g., Skumanich et al. 1997). The series of test measurements at GREGOR confirm that the routines which then are applied to the observational data will allow to determine Mueller matrices at a 10^{-3} level. This is a precondition for accurate spectropolarimetric measurements and the determination of the full magnetic vector. The high photon flux will enable to detect weak fields and plasma motions in the Solar photosphere and chromosphere down to the aspired scales of 70 km on the Sun.

Acknowledgements. The 1.5-meter GREGOR solar telescope was build by a German consortium under the leadership of the Kiepenheuer-Institut für Sonnenphysik in Freiburg with the Leibniz-Institut für Astrophysik Potsdam, the Institut für Astrophysik Göttingen, and the Max-Planck-Institut für Sonnensystemforschung in Katlenburg-Lindau as partners, and with contributions by the Instituto de Astrofísica de Canarias and the Astronomical Institute of the Academy of Sciences of the Czech Republic.

References

Balthasar, H., Bello González, N., Collados, M., et al.: 2011, in: J.R. Kuhn et al. (eds.), *Solar Polarization Workshop 6*, ASPC 437, p. 351

Beck, C., Schlichenmaier, R., Collados, M., et al.: 2005, A&A 443, 1047

Berkefeld, Th., Schmidt, D., Soltau, D., von der Lühe, O., Heidecke, F.: 2012, AN 333, 863

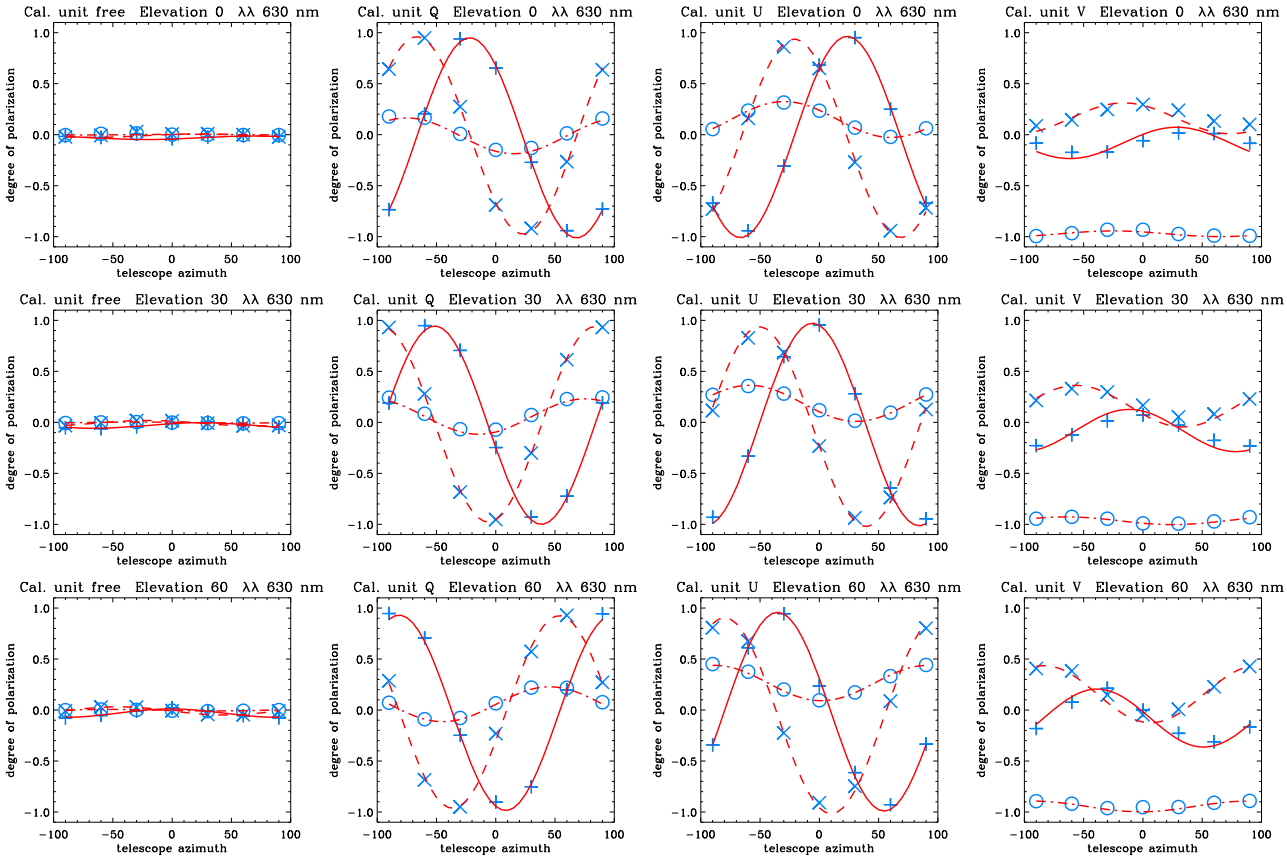

Fig. 8 (online colour at: www.an-journal.org) Results of the polarimetric measurements depending on the telescope azimuth. The rows stand for different telescope elevations. The columns stand from *left to right* for different input of light from the GPU: unpolarized light, linear polarized light Q and U, and circular polarized light V. Blue symbols represent the measurements, red curves the telescope model. Solid curves and plusses give the expected and measured Q, dashed ones and crosses the expected and measured U, and dash-dotted curves and circles the expected and measured V, respectively. Statistical errors are smaller than the symbols.

Capitani, C., Cavallini, F., Ceppatelli, G., et al.: 1989, Sol. Phys. 120, 173

Collados, M., López, R., Páez, E., et al.: 2012, AN 333, 872

Hofmann, A.: 2008, Cent. Eur. Astrophys. Bull. 32, 17

Hofmann, A., Rendtel, J., Arlt, K.: 2009, Cent. Eur. Astrophys. Bull. 33, 317

Jäger, F.W., Oetken, L.: 1963, Publ. Astrophys. Obs. Potsdam 31, 1

Lide, D.R.: 1993, *CRC Handbook of Chemistry & Physics*, 74$^{\rm th}$ edition, p. 12

Puschmann, K.G., Denker, C., Kneer, F., et al.: 2012, AN 333, 880

Samoylov, A.V., Samoylov, V.S., Vidmachenko, A.P., Perekhod, A.V.: 2004, J. Quantitative Spectroscopy & Radiative Transfer 88, 319

Sánches Almeida, J., Martínez Pillet, V.: 1992, A&A 260, 543

Schmidt, W., von der Lühe, O., Volkmer, R., et al.: 2012, AN 333, 796

Selbing, J.: 2005, Master's Thesis, Stockholm University

Skumanich, A., Lites, B.W., Martínez Pillet, V., Seagraves, P.: 1997, ApJS 110, 357

Socas-Navarro, H., Elmore, D., Asensio Ramos, A., Harrington, D.M.: 2011, A&A 531, A2

Soltau, D., Volkmer, R., von der Lühe, O., Berkefeld, Th.: 2012, AN 333, 847

van Harten, G., Snik, F., Keller, C.U.: 2009, PASP 121, 377

A Calculation of the polarimetric throughput

The Stokes-vector of the output beam $\boldsymbol{S'} = (I', Q', U', V')$ is given by $\boldsymbol{S'} = \mathbf{M} \cdot \boldsymbol{S}$ where $\mathbf{M}$ is the Mueller matrix of the polarimetric unit and $\boldsymbol{S} = (I, Q, U, V)$ is the Stokes-vector of the input beam. $\mathbf{M}$ can be composed of the matrices by the single polarizing elements and their rotations and we obtain correspondingly to Eq. (3):

$$\boldsymbol{S'} = \mathbf{G}(\varphi_2, \delta)\ \mathbf{P}(\varphi_1, k_1, k_2) \cdot \boldsymbol{S}, \tag{A1}$$

with the parameters $\varphi_1, \varphi_2, k_1, k_2$, and δ as described in Sect. 3.4.

With $k^+ = k_1 + k_2$, $k^- = k_1 - k_2$, $k^* = k_1 \cdot k_2$, $S_1 = \sin 2\varphi_1$, $C_1 = \cos 2\varphi_1$, $S_2 = \sin 2\varphi_2$, and $C_2 = \cos 2\varphi_2$, Eq. (A1) can be rewritten to

$$I' = 0.5\ (k^+ I + C_1 k^- Q + S_1 k^- U), \tag{A2}$$

$$Q' = 0.5\ (f_{iq}\ I + f_{qq}\ Q + f_{uq}\ U + f_{vq}\ V), \tag{A3}$$

where $f_{iq} = [(C_2^2 + S_2^2 \cos\delta) C_1 + S_2 C_2 (1 - \cos\delta) S_1]\ k^-$,

$$f_{qq} = (C_2^2 + S_2^2 \cos\delta)\ (k^+ C_1^2 + 2k^* S_1^2) + S_2 C_2 (1 - \cos\delta)\ S_1 C_1 (k^+ - 2k^*),$$

$$f_{uq} = (C_2^2 + S_2^2 \cos\delta)\ S_1 C_1\ (k^+ - 2k^*) + S_2 C_2 (1 - \cos\delta)\ (k^+ S_1^2 + 2k^* C_1^2),$$

$$f_{vq} = -2k^*\ S_2 \sin\delta,$$

$$U' = 0.5\ (f_{iu}\ I + f_{qu}\ Q + f_{uu}\ U + f_{vu}\ V), \tag{A4}$$

where $f_{iu} = [(S_2C_2(1-\cos\delta)\ C_1 + (S_2^2 + C_2^2\cos\delta)\ S_1]\ k^-$,

$f_{qu} = (S_2C_2(1-\cos\delta)(k^+C_1^2 + 2k^*S_1^2) + (S_2^2 + C_2^2\cos\delta)S_1C_1\ (k^+ - 2k^*)$,

$f_{uu} = (S_2C_2(1-\cos\delta)\ (S_1C_1(k^+ - 2k^*) + (S_2^2C_2^2\cos\delta)\ (k^+S_1^2 + 2k^*C_1^2)$,

$f_{vu} = 2k^*\ C_2\sin\delta$,

$$V' = 0.5\ (f_{iv}\ I + f_{qv}\ Q + f_{uv}\ U + f_{vv}\ V), \tag{A5}$$

where $f_{iv} = [S_2C_1 - C_2S_1]\ k^-\sin\delta$,

$f_{qv} = [S_2(k^+\ C_1^2 + 2k^*\ S_1^2) - (C_2S_1C_1\ (k^+ - 2k^*)]\sin\delta$,

$f_{uv} = [S_2S_1C_1(k^+\ - 2k^*) - (C_2(k^+\ S_1^2 + 2k^*\ C_1^2)]\sin\delta$,

$f_{vv} = 2k^*\ \cos\delta$.

We select the reference system in a way that it is related to the transmission axis of the polarizer. In this case, we have $\varphi_1 = 0 \longrightarrow C_1 \equiv 1,\ S_1 \equiv 0$, and the equations are reduced to

$$I' = 0.5\ \{(k^+\ I + k^-\ Q\}, \tag{A6}$$

$$Q' = 0.5\ \{(C_2^2 + S_2^2\cos\delta)\ (k^-\ I + k^+\ Q), + 2k^*\ [S_2C_2(1-\cos\delta)\ U - S_2\sin\delta\ V]\}, \tag{A7}$$

$$U' = 0.5\ \{S_2C_2(1-\cos\delta)\ (k^-\ I + k^+\ Q), + 2k^*\ [(S_2^2 + C_2^2\cos\delta)\ U + C_2\sin\delta\ V]\}, \tag{A8}$$

$$V' = 0.5\ \{S_2\sin\delta(k^-\ I + k^+\ Q) - \ 2k^*\ [C_2\sin\delta\ U + \cos\delta\ V]\}. \tag{A9}$$

